$C^+(^2P) + H_2(D_2,HD) \rightarrow CH^+(CD^+) + H(D)$. I. Reaction cross sections and kinetic isotope effects from threshold to 15 eV c.m.

Kent M. Ervin and P. B. Armentrout[a)]
Department of Chemistry, University of California at Berkeley, Berkeley, California 94720

(Received 16 December 1985; accepted 10 March 1986)

Total cross sections for the reactions of carbon(1 +) ions with isotopic molecular hydrogen (H_2, D_2, and HD) to form methyliumylidene (CH^+ and CD^+) have been measured using guided ion beam techniques. Cross sections are reported as a function of the translational energy of the reactants from the reaction threshold up to 15 eV c.m. The true cross sections are shown to rise sharply from thresholds given by the thermochemical endothermicities. Inter- and intramolecular isotope effects in the threshold region can be attributed to the different endothermicities due to vibrational zero-point energies. At higher energies, an unexpected intermolecular isotope effect is found. Thermal reaction rates (300 K) derived from the data are 1.2×10^{-16} for H_2, 2.3×10^{-17} for D_2, and 1.2×10^{-16} for HD (17% CH^+, 83% CD^+), all in units of $cm^3\ s^{-1}$.

INTRODUCTION

In 1973, Schaefer and co-workers[1] predicted that the reaction of C^+ and H_2 to form CH^+ would play a prominent part in the study of the dynamics and potential energy surfaces of simple ion–molecule reactions. More than 50 investigations related to this reaction, both experimental and theoretical, have appeared in the scientific literature since that time bearing out the accuracy of this prediction. The $C^+ + H_2$ reaction has evoked continuing interest for several reasons. First, it has become a model system for the experimental study of the kinetics and dynamics of endothermic ion–molecule reactions. Second, the $C^+ + H_2$ system involves several potential energy surfaces. The features of these surfaces and the interactions among them must be known for a detailed understanding of the reaction dynamics. *Ab initio* calculations[1–4] of the potential energy surfaces have complemented the experimental studies. Third, the reaction has served as a test case for theoretical treatments of ion–molecule reactions such as phase space theory[5–7] and classical trajectory calculations.[8,9] Finally, the reaction is significant in astrophysics due to the abundance of CH^+ in interstellar space. The hydrogen atom transfer reaction is a possible source of CH^+ under certain interstellar conditions.[10]

While this system has been studied a great deal, the integral reaction cross sections are still not well characterized. In a preliminary note,[11] we showed that previous determinations[12–14] of the threshold behavior of the cross section were seriously in error due to experimental difficulties and errors of interpretation. In this work, we present more complete measurements of the total cross section for $C^+(^2P) + H_2 \rightarrow CH^+ + H$ and also the reactions with D_2 and HD. Guided ion beam techniques[15] permit precise determinations of integral reaction cross sections with good energy resolution. The cross sections are examined as a function of the translational energy of the reactants from the threshold to about 15 eV c.m. Energy-dependent reaction rates and thermal reaction rates are also derived from the data. The quality of the data and the new information on the kinetic isotope effects make possible detailed comparisons to theoretical treatments of this reaction. In a companion article (II),[16] we compare the results to a statistical phase space theory treatment.

REACTION CHANNELS AND THERMOCHEMISTRY

Early investigations of the $C^+ + H_2 \rightarrow CH^+ + H$ reaction were hampered by uncertainties in the thermochemistry of the reaction.[17] Fortunately, recent spectroscopic measurements[18–21] and theoretical calculations[22] have provided reliable bond energies and molecular constants for the ground and lower excited electronic states of the CH^+ product. The ground state reaction channels and their endothermicities are

$$C^+(^2P_{1/2}) + H_2(^1\Sigma^+) \rightarrow CH^+(X\,^1\Sigma^+) + H(^2S), \quad \Delta H^\circ_0 = 0.398 \pm 0.003\ \text{eV}, \tag{1}$$

$$C^+(^2P_{1/2}) + D_2(^1\Sigma^+) \rightarrow CD^+(X\,^1\Sigma^+) + D(^2S), \quad \Delta H^\circ_0 = 0.430 \pm 0.005\ \text{eV}, \tag{2}$$

$$C^+(^2P_{1/2}) + HD(^1\Sigma^+) \rightarrow CH^+(X\,^1\Sigma^+) + D(^2S), \quad \Delta H^\circ_0 = 0.434 \pm 0.005\ \text{eV}, \tag{3a}$$

$$\rightarrow CD^+(X\,^1\Sigma^+) + H(^2S), \quad \Delta H^\circ_0 = 0.388 \pm 0.005\ \text{eV}. \tag{3b}$$

The thermochemical quantities are derived from diatomic dissociation energies listed in Table I. The enthalpies listed are for 0 K, i.e., they are not corrected for the internal energies of the reactants. Due to the small endothermicity of these reactions, both the rotational energy of the hydrogen molecule, 0.024 eV, and the energy of the $C^+(^2P_{3/2})$ spin-orbit state, 0.008 eV, can be significant in the threshold region.

[a)] NSF Presidential Young Investigator 1984–89.

 0021-9606/86/126738-12$02.10

As the $C^+(^2P) + H_2$ reactants approach, three doubly degenerate potential energy surfaces are formed. Calculations of the potential energy surfaces[1-4] have shown that two of the three surfaces either have large barriers or lead to electronically excited states of the products. The third surface, for most orientations, has a barrier-less pathway to the CH_2^+ potential well (about 4 eV deep) and on to products. This surface allows the reaction to proceed at the thermochemical threshold, but only in one-third of the collisions (assuming a statistical initial population of the reactant states). The potential energy surfaces are considered in more detail in the companion paper.[16]

Formation of excited state products is possible at the higher energies of this study. While the mass spectrometric detection employed in the guided beam technique is insensitive to the internal state of the product ions, features in the integral cross sections or isotopic branching ratios might be expected to correlate with the onset of these channels. Electronically excited product channels include

$$C^+(^2P_{1/2}) + H_2(^1\Sigma^+) \rightarrow CH^+(a\,^3\Pi) + H(^2S), \quad \Delta H_0^\circ = 1.54 \pm 0.1 \text{ eV}, \tag{4}$$

$$\rightarrow CH^+(A\,^1\Pi) + H(^2S), \quad \Delta H_0^\circ = 3.327 \pm 0.003 \text{ eV}, \tag{5}$$

$$\rightarrow CH(^2\Pi) + H^+(^1S), \quad \Delta H_0^\circ = 3.37 \pm 0.1 \text{ eV}, \tag{6}$$

$$\rightarrow CH^+(b\,^3\Sigma^-) + H(^2S), \quad \Delta H_0^\circ = 5.1 \pm 0.1 \text{ eV}. \tag{7}$$

The singlet–triplet splitting used to derive these endothermicities has not been measured and is taken from theoretical calculations (see Table I).

EXPERIMENTAL METHODS

The experimental techniques and data reduction procedures used in this study have been described in detail elsewhere,[15] so only salient features are described here.

Guided ion beam apparatus

The guided ion beam technique was first developed by Teloy and Gerlich[23] and has been successfully exploited to study a variety of ion–molecule reactions.[24] These studies have demonstrated the ability of the guided beam method to measure accurate integral cross sections of ion–molecule reactions as a function of translational energy from near thermal to several hundred electron volts ion energy.

The guided ion beam apparatus utilizes a radio-frequency octopole "pipe" to direct a beam of ions with a variable kinetic energy through a static gas collision cell. Ions may be produced by any of several types of ion sources. The ions are focused into a beam, mass selected in a magnetic sector, and injected into the octopole beam guide at the desired kinetic energy. The octopole traps scattered ions, allowing 4π collection of products with near 100% efficiency. The ions are extracted from the octopole, mass analyzed with a quadrupole mass spectrometer, and counted using a secondary electron scintillation detector and pulse counting electronics. The reaction cross sections are derived directly from the measured reactant and product ion intensities, the measured gas cell pressure, and the estimated reaction path length. Due to the trapping characteristics of the octopole, the collection efficiency for scattered products is superior to conventional ion beam/gas cell experiments. A prime advantage of the method over other techniques for studying thermal and hyperthermal ion–molecule reactions (e.g., flow/drift tube and ion cyclotron resonance experiments) is that the kinetic energy of the reactants is routinely and precisely determined and has a well-characterized distribution. The ion beam kinetic energy is determined to within ± 0.1 eV lab (± 0.014 eV c.m. for $C^+ + H_2$) by utilizing the octopole itself as a retarding energy analyzer.[15] The width of the ion beam energy distribution is also measured by the retarding energy analysis. Our previous description[15] contains further details concerning the guided ion beam apparatus. The only instrumental changes for the present experiments are the use of a higher octopole frequency (13 vs 7 MHz), which is appropriate for efficient trapping of lighter ions, and the ion source which is described below.

TABLE I. Bond dissociation energies D_0°(eV).

$CH^+(X\,^1\Sigma^+)$	$\rightarrow C^+(^2P_{1/2}) + H$	4.080 ± 0.003[a]
$CD^+(X\,^1\Sigma^+)$	$\rightarrow C^+(^2P_{1/2}) + H$	4.126 ± 0.005[b]
$CH^+(a\,^3\Pi)$	$\rightarrow C^+(^2P) + H$	2.94 ± 0.1[c]
$CH^+(A\,^1\Pi)$	$\rightarrow C^+(^2P_{3/2}) + H$	1.159 ± 0.003[a]
$CH^+(b\,^3\Sigma^-)$	$\rightarrow C(^3P) + H^+$	1.7 ± 0.1[d]
$CH(^2\Pi)$	$\rightarrow C(^3P) + H$	3.465[c]
$H_2(^1\Sigma^+)$		4.4781[c]
$HD(^1\Sigma^+)$		4.5138[c]
$D_2(^1\Sigma^+)$		4.5563[c]

[a] Reference 19.
[b] Calculated from $D_0^\circ(CH^+\,^1\Sigma^+)$ and vibrational frequencies tabulated in Ref. 16.
[c] K. P. Huber and G. Herzberg, *Constants of Diatomic Molecules* (Van Nostrand Reinhold, New York, 1979).
[d] From $T_e(a\,^3\Pi \rightarrow b\,^3\Sigma^-) = 3.58$ eV, Ref. 18.

$C^+(^2P)$ ion source

In our preliminary work on this reaction,[11] we utilized a conventional electron impact ionization source for producing C^+ ions from CO. To insure that only $C^+(^2P)$ ground state ions were produced, a low electron energy (25 eV or lower) was used. The appearance potential for forming $C^+(^2P)$ (and O^-) from CO is ~ 21 eV[25] and the first electronically excited state of the carbon ion, $C^+(^4P)$, lies 5.3 eV above the ground state.[26] Here we use a high pressure coaxial ion source modeled after the design of Bowers and coworkers,[27] which gives higher ion intensities without producing excited carbon ions. Electrons are injected into a drift region which contains a relatively high pressure (0.1 to 1 Torr) of CO gas. The ions formed by electron impact ionization undergo numerous collisions with the CO bath gas while being drawn through the cell by a weak electric field.

These collisions and resulting sequences of ion–molecule reactions serve to thermalize the ions. The ions drift to the end of the cell and through an exit aperture. Here they enter the ion beam focusing and mass selection region of the guided ion beam apparatus described above.

The physical design of the drift cell ion source is similar to that described by Bowers and co-workers.[27] The electron injection aperture is 0.40 mm in diameter. The exit aperture is also circular (rather than a slit as in Ref. 27) and has the same diameter. The length of the drift region is 20 mm. A small three-element lens is placed between the electron filament and the electron injection aperture for focusing electrons into the drift region. The entire assembly stacks together on 0.062 50 in. diameter precision ruby balls to insure proper alignment of the filament, apertures, and field guard rings.

Ion source conditions are optimized to produce intense beams of ground state carbon ions with narrow kinetic energy distributions. An electron injection energy of 40 to 50 eV is used. Typical drift conditions are a CO pressure of 200 mTorr and a drift potential of 2 V. The drift cell is kept near room temperature by flowing air or water through cooling ducts in the source block. Typical ion beam energy distributions are nearly Gaussian and are characterized by the widths $W(50\%) = 0.25$ eV, $W(10\%) = 0.50$ eV, and $W(1\%) = 1.0$ eV.

Since the $C^+(^4P) + H_2 \rightarrow CH^+ + H$ reaction is exothermic and rapid, the presence of a low-energy exothermic channel in the $C^+ + H_2$ reaction cross section is an indicator of excited states in the C^+ ion beam. The low-pressure electron impact source produces a sizable fraction of excited C^+ for electron energies greater than 30 eV, resulting in a strong exothermic channel in the observed cross section for reaction with H_2. In contrast, raising the electron energy in the drift cell source up to 100 eV produces no change in the threshold region of the cross section. This confirms that the beam contains only ground state $C^+(^2P)$ ions. The populations of the spin-orbit states of $C^+(^2P_J)$ are not known experimentally, but are presumed to be statistical ($^2P_{3/2}$:$^2P_{1/2} = 2{:}1$).

Energy deconvolution

The experimental cross sections are broadened due to the random thermal motion of the target gas. Chantry[28] derived the convolution function for the case of a monoenergetic ion beam and Lifshiftz *et al.*[29] extended the treatment to include the ion beam energy spread. Since the beam guide experiments are carried out under single collision conditions, specific interactions between the ions and the target gas (e.g., ion mobilities) need not be considered. The width of the energy distribution increases as $E^{1/2}$ with increasing energy, but in the limit of zero ion energy the distribution is characterized by the Boltzmann distribution of the target gas. Thus, the relative energy spread ($\Delta E/E$) is larger for low kinetic energies.

We have previously described procedure for extracting the true cross section behavior from observed effective cross sections.[15] This entails forward convolution of a trial excitation function with the known experimental energy distribution for comparison with the data. The chosen function is a power law of the form

$$\begin{aligned} \sigma(E) &= \sigma_0 \cdot (E - E_T)^n / E^m \qquad \text{if } E > E_T, \\ \sigma(E) &= 0 \qquad\qquad\qquad\qquad\quad \text{if } E \leqslant E_T, \end{aligned} \tag{8}$$

where $\sigma(E)$ is the cross section, E is the relative kinetic energy of the reactants, E_T is the threshold energy, and σ_0, n, and m are either derived from a theoretical model or are adjustable parameters. This function is physically reasonable but is also flexible enough to avoid biasing the results to a large degree. Theoretical cross sections of this form have been derived from several reaction models, giving values for the powers of $n = m = 1$ (line-of-centers model[30]); $n = 0.5$, $m = 1$ (ion-induced dipole model[31]); and $m = 1$, n varies (transition state theory of translationally driven reactions[32]). Other entirely empirical functional forms have also been used[7(b),28]; however, Eq. (8) can mimic those if n and m are allowed to vary freely. The variable parameters are optimized to fit the data after convolution of the trial function using a least squares analysis. With due care in the fitting procedure, the form of the true cross section can be established within fairly tight limits.

We use the exact convolution integral of Lifshitz *et al.*,[29] which includes broadening from both the thermal motion of the target gas and the ion beam energy spread.[33] It should be noted that the high-energy approximations to the convolution functions given by both Chantry[28] and Lifshitz *et al.*[29] are not valid at the energies of the threshold region for the $C^+ + H_2$ system.[34] All convolutions are calculated numerically using adaptive integration techniques.[35]

REACTION CROSS SECTIONS

Cross sections for reactions 1, 2, and 3 are shown in Figs. 1, 2, and 3, respectively. The data represent averages of measurements taken over a period of about one year under varying instrumental conditions. A total of 26 scans over various energy ranges were averaged for reaction (1), 13 for reaction (2), and 11 for reaction (3). The density of measurements is greater in the low-energy threshold region. The error bars in Figs. 1–3 are $\pm$ 1 standard deviation in the averaged values, reflecting all experimental and instrumental uncertainties but not systematic errors. The relative values of the cross section as a function of energy for a single reaction have an uncertainty of about 5%. The uncertainties of the absolute magnitudes are limited by our ability to measure the gas cell pressure and to estimate the reaction path length. The absolute errors are expected to be within $\pm$ 20%.

An expanded, semilogarithmic plot of the cross sections in the threshold region for all for isotopic reactions is shown in Fig. 4. The total reaction cross sections rise from apparent thresholds of about 0.1 eV c.m. These apparent threshold energies are significantly lower than the thermochemical endothermicities of ~0.4 eV. The primary reasons for this is the energy broadening caused by the random motion of the hydrogen gas in the collision cell. The combination of a low reaction threshold and light target mass makes the experimental energy broadening particularly prominent (and troublesome) for this system. The widths of the experimental energy distributions are approximately $0.50E^{1/2}$

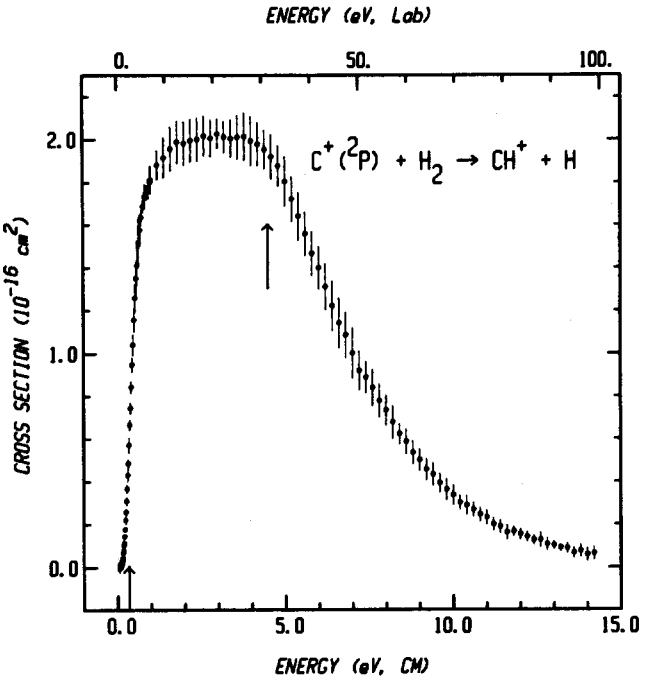

FIG. 1. Cross section for reaction (1) as a function of the carbon ion kinetic energy in the laboratory frame (upper scale) and the center-of-mass frame (lower scale). Each point represents the average of several determinations. Vertical error bars indicate $\pm$ 1 standard deviation. Arrows indicate the thermochemical threshold energy, $\langle E_T \rangle = 0.369$ eV, and the bond dissociation energy of H_2, 4.48 eV.

(FWHM) for reaction 1, $0.47E^{1/2}$ for reaction (2), and $0.48E^{1/2}$ for reaction (3), where E is nominal energy in the center-of-mass frame.[15] At the 0.4 eV threshold, the FWHM is about 0.3 eV.

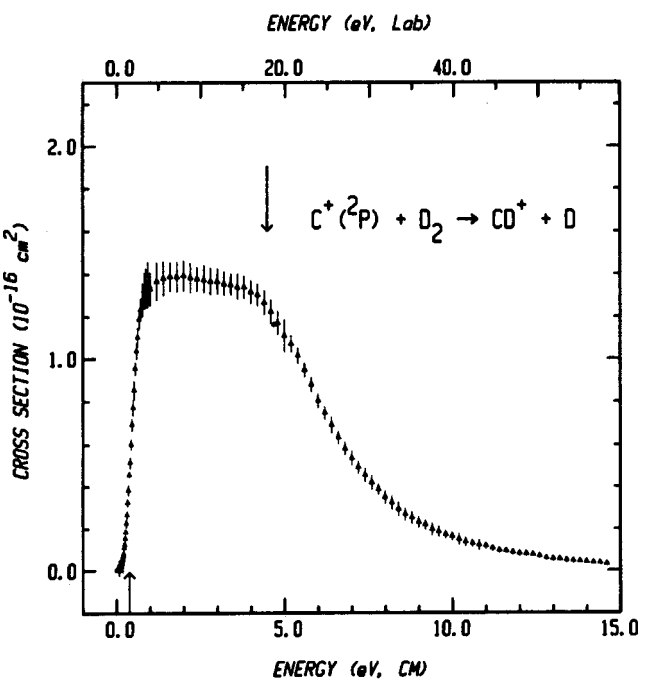

FIG. 2. Cross section for reaction (2) as a function of the carbon ion kinetic energy in the laboratory frame (upper scale) and the center-of-mass frame (lower scale). Each point represents the average of several determinations. Vertical error bars indicate $\pm$ 1 standard deviation. Arrows indicate the thermochemical threshold energy, $\langle E_T \rangle = 0.400$ eV, and the bond dissociation energy of D_2, 4.56 eV.

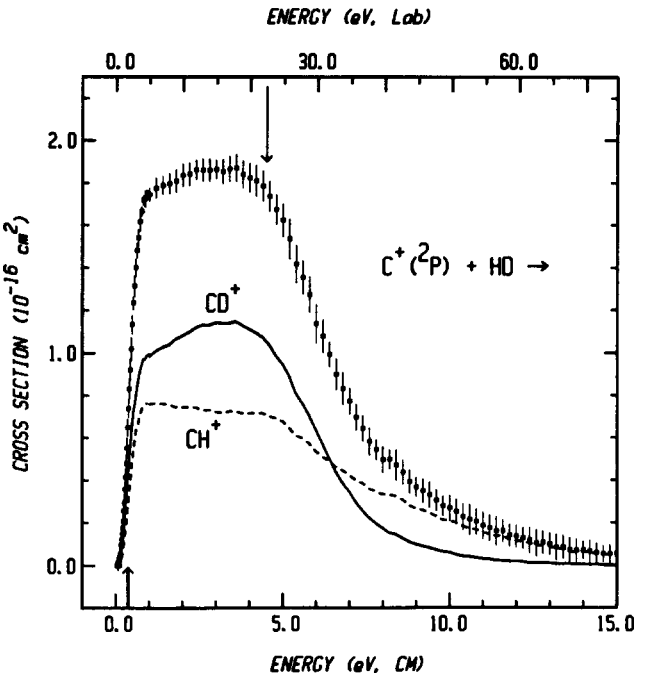

FIG. 3. Cross section for reaction (3) as a function of the carbon ion kinetic energy in the laboratory frame (upper scale) and the center-of-mass frame (lower scale). Each point represents the average of several determinations of the total reaction cross section. Vertical error bars indicate $\pm$ 1 standard deviation. The dashed line gives the cross section for reaction (3a), formation of CH^+, and the solid line gives the cross section for reaction (3b), formation of CD^+. Arrows indicate the thermochemical threshold energy, $\langle E_T \rangle = 0.404$ eV for CH^+ and $\langle E_T \rangle = 0.359$ eV for CD^+ (superimposed on this scale), and the bond dissociation energy of HD, 4.51 eV.

Following the threshold region, a remarkably flat plateau in the cross sections extends up to about 4.5 eV. This energy is the threshold for dissociation of the $CH^+(CD^+)$ product,

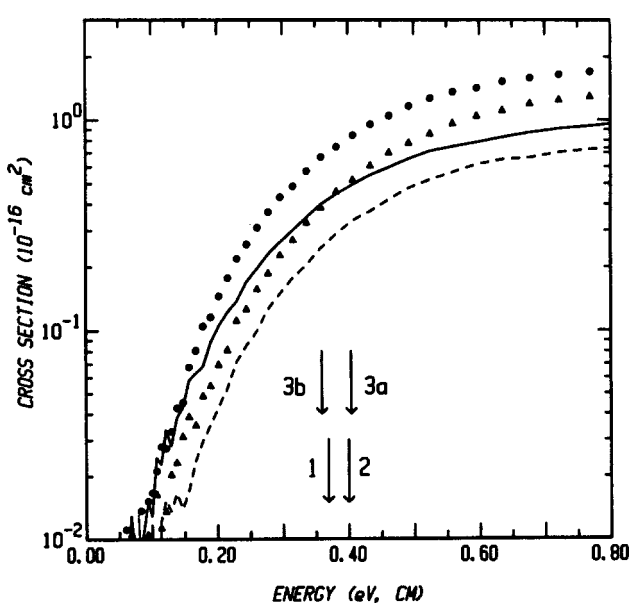

FIG. 4. Cross sections for reactions (1) (circles), (2) (triangles), (3a) (dashed line), and (3b) (solid line) on an expanded semilogarithmic scale in the threshold region. The data are the same as in Figs. 1, 2, and 3. Arrows indicate the thermochemical threshold energies $\langle E_T \rangle$ for each of the reactions.

$$C^+ + H_2 \rightarrow C^+ + H + H, \quad \Delta H_0^\circ = 4.48 \text{ eV}, \qquad (9)$$

and the cross sections decrease above this point. This extended plateau region is somewhat atypical for endothermic ion–molecule reactions and is due in part to the large separation between the reaction threshold and the onset of process (9).

Our preliminary report[11] presented in the threshold region of reaction (1). The current results near the threshold (Figs. 1 and 4) are similar but have a much better signal-to-noise ratio and slightly less energy broadening near the apparent threshold. The latter is primarily due to instrumental improvements[15] undertaken since the preliminary study which have allowed more precise determination of the ion energy through better injection of ions into the octopole trap at low energies. Much care was taken in the present experiments to determine the ion beam energy as accurately as the instrumentation allows, i.e., within ± 0.1 eV lab by retarding energy analysis.

Comparison to literature

Several measurements of the integral cross section in the threshold region have been reported,[12–14] beginning with the very first observation of an endothermic ion–molecule reaction by Maier.[12] All of these experiments suffered from difficulties in establishing an accurate collision energy scale. Following Maier's example, later investigators[13,14] "corrected" the energy scale to match the apparent experimental threshold of ~ 0.1 eV with the thermochemical endothermicity of ~ 0.4 eV. The precise ion energy determination afforded by the guided beam technique obviates the need for such corrections. In our previous note[11] on the threshold region of reaction (1), we showed that these energy scale corrections were in error. Using the uncorrected experimental energy scales of the earlier work[12–14] yields greatly improved agreement with our threshold data.[36]

At higher energies the present results also generally agree with the literature within the uncertainty of the earlier experiments,[12–14] although the fall-off behavior of the cross sections tends to differ from instrument to instrument. This is not surprising considering that in conventional beam/gas experiments the product collection probability is strongly dependent on the angle of scattering. Near the threshold, the products cannot be widely scattered due to the lack of available energy, but at higher energies the products can have broad angular and energy distributions. The trapping properties of the octopole in the guided beam apparatus serve to collect these scattered ions more efficiently.

Additional data on these systems are contained in more recent, unpublished work by Cahnbley[37] and Gerlich.[38] These studies came to our attention after the experimental portion of this work was nearly complete. Cahnbley used the guided beam apparatus of Teloy and Gerlich[23] to obtain cross sections for reactions (1) and (2). Both the magnitude and relative shape of the excitation functions are in generally good agreement with the data reported here. Deviations between the two sets of data are within experimental error below 3 eV c.m., but are somewhat larger in the high energy region. Gerlich[38] very recently reported cross section measurements for reaction (1) up to 0.7 eV c.m. using a guided ion beam apparatus which uses time-of-flight methods to determine the ion energy to ± 10 meV. These results are 12% larger than ours in absolute magnitude,[39] but have almost identical relative threshold behavior. A detailed comparison shows, however, that our low-energy results are shifted to slightly lower energies relative to Gerlich's. Differences in energy broadening attributable to different target gas temperatures (305 ± 10 in this work; 320 and 380 K in Ref. 38) were taken into account. The remaining deviation in energies, about 0.1 eV lab or 0.014 eV c.m. for reaction (1), is at the outside limit of the uncertainty of our energy determination. Rather crude time-of-flight measurements on our apparatus reported previously had an uncertainty of ± 0.15 eV, but tended to give energy values about 0.1 eV lower than those determined by the more precise retarding energy analysis.[15] It is possible that energy shifts in this direction in the retarding potential analysis could be caused by potential barriers produced by imperfections or foreign particles on the octopole rods.[40] While such an energy discrepancy is small for most purposes, it can affect the deconvolution of the effective cross section when trying to extract the true threshold behavior. Therefore, we have explicitly considered energy errors of ~ 0.1 eV lab in determining uncertainties in the fits of model cross sections to the data.

KINETIC ISOTOPE EFFECTS

Intermolecular isotope effects

The relative behavior of the H_2, D_2, and total HD excitation functions as a function of energy is very similar (Figs. 1 to 3), except at the threshold where the zero point energy differences among reactions (1), (2), (3a), and (3b) produce energy shifts. These threshold shifts are obvious in the raw data (Fig. 4) despite the energy broadening.

The absolute magnitudes of the cross sections of the H_2, HD, and D_2 reactions are reproducibly different. At 2.0 eV c.m., an energy which is representative of the plateau region of the cross section, $\sigma_2(CD^+)/\sigma_1(CH^+) = 0.7 \pm 0.1$ and $\sigma_3(\text{total})/\sigma_1(CH^+) = 0.9 \pm 0.1$, where the subscripts refer to reactions (1), (2), or (3). While the experimental uncertainty in the absolute magnitudes of cross sections measured on the guided beam apparatus is $\pm 20\%$, the relative values of cross sections for different reactions are expected to have uncertainties of only 5%–10%. The product collection efficiency of the guided beam method is generally excellent, but small systematic errors in collection or detection of different product ions cannot be completely ruled out. However, variation of several instrumental parameters which could affect the collection efficiency, such as the octopole trapping potential and quadrupole mass resolution, did not alter the results.

Independent confirmation of the intermolecular isotope effect for the H_2 and D_2 reactions is contained in two unpublished studies. Fennelly[14] investigated reactions (1) and (2) using a beam/gas cell instrument with partial reactant ion mass selection. While the results are rather scattered, the cross section for reaction (1) is consistently larger than for reaction (2). More unambiguous are measurements of the cross sections for reactions (1) and (2) by Cahnbley,[37] who finds that $\sigma_2(CD^+)/\sigma_1(CH^+)$ is 0.75 to 0.80 in the plateau

region (compared to our value of 0.7 ± 0.1). Like the present apparatus, the instrument used by Cahnbley[37] incorporates an octopole ion beam guide, but has a quite different product mass analyzer and ion detector arrangement. The fact that three different instruments show the same trend in the intermolecular isotope effect provides strong evidence for its existence. The only other study where both H_2 and D_2 reaction cross sections were measured is the early work of Koski and co-workers,[13(a)] which reported equal magnitudes for the two isotopic variants.

A strong $H_2/D_2/HD$ intermolecular isotope effect is not expected *a priori*. For instance, phase space theory predicts that the total cross sections are within 5%–10% except near threshold.[7(a),16] No model has been found which satisfactorily explains this effect. We note that the 1.0:0.9:0.7 ratio of the total cross sections for the H_2, HD, and D_2 reactions, respectively, matches within experimental error the 1.0:0.86:0.76 ratio of $(1/\mu)^{1/2}$ for the three systems, where μ is the reduced mass of the system in the entrance channel. This suggests that the intermolecular isotope effect may scale with the velocities $[v = (2E/\mu)^{1/2}]$ in the atom–diatom coordinate.

Intramolecular isotope effect

Figure 3 presents the total cross section for $C^+ + HD$, along with the individual cross section for forming CH^+ and CD^+, reactions (3a) and (3b), respectively. The intramolecular isotope effect is also shown as the branching ratio $\sigma_3(CH^+)/\sigma_3(\text{total})$ in Fig. 5. Because systematic errors in the total cross sections generally cancel, the experimental uncertainty of the isotope branching ratio is no more than 5% except in regions where one channel is very small. To our knowledge, the only previous measurement of the isotopic branching ratio for reaction (3) is the unpublished work Fennelly *et al.*[14] The agreement between the observations is well within experimental uncertainties.

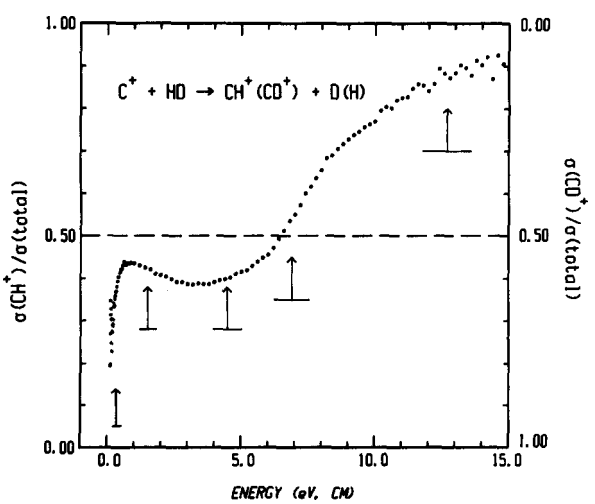

FIG. 5. Isotopic branching ratio for reaction (3) presented as the fraction of CH^+ product, $\sigma(CH^+)/[\sigma(CH^+) + \sigma(CD^+)]$, left ordinate, and the corresponding fraction of CD^+ product, right ordinate. The abscissa is the carbon ion kinetic energy in the center-of-mass frame. Arrows indicate, from left to right, the threshold energy of the ground state reaction, the threshold for making $^3\Pi$ CH^+ products [reaction (4)], the bond dissociation energy of HD [threshold of process (9)], and the spectator stripping critical energies for CD^+ (6.9 eV) and for CH^+ (12.7 eV). Horizontal bars indicate one FWHM of the experimental energy distribution at each nominal center-of-mass energy.

The CD^+ channel has a lower threshold than the CH^+ channel due to the 0.046 eV difference in zero-point vibrational energies of CD^+ and CH^+. The prominent sharp rise in the branching ratio at the threshold (Fig. 5) is clearly due to this difference in endoergicity. The branching ratio $\sigma_3(CH^+)/\sigma_3(\text{total})$ reaches a maximum of ~0.43 at about 1 eV, then decreases with increasing energy to ~0.38 between 3 and 4 eV. Near 4.5 eV, the threshold for the collisional dissociation of HD analogous to process (9), the isotope branching ratio begins to increase. This indicates that the hydride product is favored in the energy region where product dissociation mechanisms become important. This is typical behavior for reactions of atomic ions with HD.

THRESHOLD REGION

Empirical deconvolution

In order to obtain an empirical description of the true threshold behavior, the trial function, Eq. (8), is convoluted with the experimental energy distributions and the adjustable parameters are optimized to fit the data, as discussed above. The threshold energy is fixed at $\langle E_T \rangle = \Delta H_0^\circ - \langle E_{\text{rot}} \rangle - \langle E_{\text{so}} \rangle$, where $\langle E_{\text{rot}} \rangle$ is the mean rotational energy of the hydrogen molecule and $\langle E_{\text{so}} \rangle$ is the mean spin-orbit energy of $C^+(^2P_J)$. Assuming a statistical population of $J = 1/2$ and $J = 3/2$, $\langle E_{\text{so}} \rangle$ is only 5 meV and therefore is not a large contribution to the available energy, although spin-orbit effects might influence the reactivity. At room temperature, hydrogen is in its ground vibrational state, but the mean rotational energy of hydrogen is about $k_B T$ or 0.024 eV. This produces a small but significant energy shift in the threshold. Using the average value $\langle E_{\text{rot}} \rangle$ gives cross sections which are virtually identical after convolution to those obtained by calculating the cross section as an explicit sum over the individual rotational states of H_2 with the same trial function form, i.e.,

$$\sigma(E) = \sigma_0 \cdot \sum_J f(J) \cdot [E - E_T(J)]^n / E^m, \qquad (10)$$

where $f(J)$ is the fractional population of level J and $E_T(J) = \Delta H_0^\circ - \langle E_{\text{so}} \rangle - E_{\text{rot}}(J)$. Subtracting the diatomic rotational energy from the threshold value assumes that rotational energy and translational energy are equally effective in promoting reaction.[41] In the absence of experiments pertaining to the rotational dependence of the cross sections, this assumption seems reasonable.

For purposes of determining the threshold behavior, Eq. (8) is optimized to fit the data up to 1.0 eV. This energy is about one FWHM of the energy distribution below the threshold for formation of the first electronically excited state of CH^+, reaction (4), and thus avoids possible effects due to the onset of that process.

Two functions commonly used to model reaction thresholds, linear ($n = 1$, $m = 0$) and line-of-centers ($n = m = 1$) forms, fail utterly to match the data. The experimental threshold behavior of the apparent cross section

as a function of energy can be accounted for only by a true cross section which rises very sharply from the thermochemical threshold. A model[31] for the threshold behavior of endoergic ion–molecule reactions derived from microscopic reversibility arguments and based on the long range ion–induced dipole potential predicts $n = 0.5$ and $m = 1$. This form was used in our preliminary work[11] to demonstrate that a simple model could be used to give a reasonable reproduction of the data without resorting to the energy scale "corrections" used by earlier researchers. Although it exhibits the necessary sharp rise at the threshold and mimics the general behavior of the experimental cross section near the threshold, the fit is far from perfect—especially when compared to the present data which have less scatter. Better fits are obtained by allowing n or m to vary freely. Table II lists the best empirical fits to the data for reactions (1), (2), (3a), and (3b) using various forms of Eq. (8) as the trial function. The best overall fits used $m = 1.0$ (fixed) and $n = 0.59$ to 0.68 (optimized). This was the only form which gave reasonable fits *and* had similar relative values of the optimized exponents for all four isotopic reactions (Table II). The threshold region of reaction (1) with this trial function, is depicted in Fig. 6(a) on a linear scale, which emphasizes the high-energy region, and in Fig. 6(b) on a semilogarithmic scale, which emphasizes the low-energy tail. The other trial functions, for which m as well as n was optimized, result in only marginally better reproductions of the data. The empirical threshold fits to reactions (2), (3a), and (3b) are of similar quality.

Threshold behavior

The sharp rise in the reaction probability at the thermochemical threshold energies confirm that there is at least one potential energy surface which leads to products without a barrier. This is consistent with *ab initio* calculations, which indicate that one of the three entrance channel surfaces has no barrier.[1–4] The $n \approx 0.6$ to 0.7, $m = 1$ form of the empirical excitation function is quite similar to the $n = 0.5$, $m = 1$ form predicted by the ion–induced dipole model for endothermic reactions.[31] The controlling factor in this model is the ability of the products to surmount the centrifugal barrier on the effective long range potential in the exit channel. The large change in reduced mass in going from reactants to products and the reduction in energy due to the endothermicity means that the exit channel centrifugal barrier is the greatest constraint in these systems.

For all of the reactions, good empirical fits to the data cannot be obtained without subtracting the diatom rotational energy from the 0 K threshold energy. Further, slightly lower threshold energies (10–30 meV) would give better fits to the low-energy tail of the apparent threshold than that

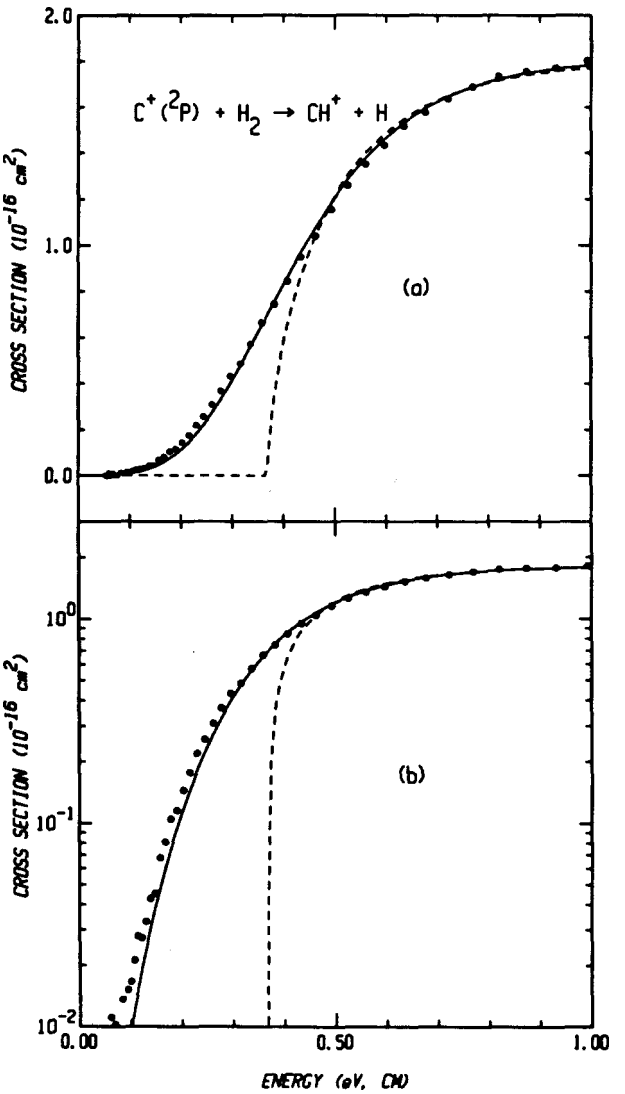

FIG. 6. Empirical fit to the threshold region of reaction (1) on a linear scale (a) and a semilogarithmic scale (b). Circles give the experimental cross sections as a function of kinetic energy of reactants. The dashed line gives the model function, Eq. (8), with $\sigma_0 = 2.42 \times 10^{-16}$ cm^2 eV$^{0.32}$, $E_T = 0.369$ eV, $n = 0.68$, and $m = 1.0$. The solid line is the same function convoluted with the experimental energy distributions.

TABLE II. Threshold fits.[a]

n	m	$\langle E_T \rangle$(eV)	$\sigma_0(10^{-16}\,\text{cm}^2\,\text{eV}^{m-n})$
(1) $C^+ + H_2 \rightarrow CH^+ + H$			
0.68 ± 0.05	1.0	0.369	2.43
0.44 ± 0.1	n	0.369	2.20
0.38 ± 0.2	0.30 ± 0.2	0.369	2.15
(2) $C^+ + D_2 \rightarrow CD^+ + D$			
0.67 ± 0.1	1.0	0.400	1.92
0.45 ± 0.2	n	0.400	1.73
0.50 ± 0.3	0.59 ± 0.3	0.400	1.78
(3a) $C^+ + HD \rightarrow CH^+ + D$			
0.59 ± 0.1	1.0	0.404	1.03
0.32 ± 0.2	n	0.404	0.91
0.27 ± 0.4	0.17 ± 0.4	0.404	0.88
(3b) $C^+ + HD \rightarrow CD^+ + H$			
0.67 ± 0.1	1.0	0.359	1.31
0.40 ± 0.2	n	0.359	1.18
0.14 ± 0.4	-0.15 ± 0.4	0.359	1.08

[a] Parameters refer to Eq. (8) in the text. Underlining indicates parameters constrained to the given value. Error limits indicate range of possible values considering the ± 0.1 eV lab uncertainty in the experimental energy scale.

shown in Fig. 6. While this may partially reflect an energy scale error, the ± 0.1 eV lab uncertainty discussed earlier, this observation indicates that the higher populated rotational states of hydrogen are at least as reactive as the ground state. A degree of rotational enhancement would also be consistent with the results, although there is no definitive evidence for this. In a review of quasiclassical trajectory studies, Sathyamurthy[42] notes that rotational energy generally enhances reaction for mechanisms involving complex formation due to the presence of a deep potential well. On the other hand, phase space theory results for this system indicate only a small rotational enhancement other than the lowering of the threshold energy.[5,16]

Threshold energy determination

The $C^+ + H_2$ system allows a test of whether accurate threshold values can be determined using the empirical modelling procedure assuming the actual endothermicities were not known. Unfortunately, in this case if E_T as well as n and m in Eq. (8) are freely optimized to fit the data, the resulting threshold values are 0.05 to 0.15 eV lower than the known endothermicities. This result provides a caveat concerning the use of experimental thresholds to determine endothermicities of ion–molecule reactions. Namely, careless or naive application if an empirical model function can in some cases give grossly incorrect values for the actual threshold. This is particularly true for the $C^+ + H_2$ system because the low threshold energy, the steep rise in the excitation function at the threshold, and the heavy-on-light mass combination all cause extensive experimental energy broadening which obscures the true threshold behavior. The inappropriate energy corrections applied by early investigators of this reaction demonstrate the extent to which these factors can mislead. On the other hand, if the shape of the threshold function is known from comparison with similar systems which have been previously examined or from theoretical treatments *and* the data are of high quality, judicious use of the deconvolution procedure can give accurate values for thermochemical quantities. Previous work on other systems which do not present the special difficulties of $C^+ + H_2$, for example the isovalent $Si^+ + H_2$ reaction,[24(c)] has shown that endothermicities can be determined from thresholds using ion beam guide methods with precision rivaling spectroscopic measurements.

In the case of reactions (1) to (3), phase space theory quite accurately models the threshold behavior. As described in paper II, endothermicities obtained by using phase space theory as a semiempirical model with the threshold energy as an adjustable parameter are within 40 meV of the expected values.

PLATEAU REGION

The total cross section for all three isotopic reactions is flat from 1 up to 4.5 eV. According to the simple ion–induced dipole model for endothermic reactions [$n = 0.5$ and $m = 1$ in Eq. (8)],[31] the cross sections would be expected to decline following the initial threshold rise due to the declining orbiting collision (Langevin) cross section. The Langevin collision cross section, which predicts $\sigma(E) \propto E^{-1/2}$, is not valid at high energies since the collision cross section eventually tends toward the hard sphere cross section. For this reaction, the estimated hard sphere cross section is $\sim 3.5 \times 10^{-16}$ cm^2. The Langevin cross section is larger than that until about 18 eV. Furthermore, the total cross sections for reactions (1), (2), and (3) are much smaller than either the Langevin or the hard sphere collision cross section. This means that other factors, such as the energy barriers on some of the entrance channel surfaces and angular momentum constraints in the exit channel, limit the reaction probability for a given collision. As the energy increases, new electronic and rovibrational product channels become accessible. This may increase the reaction probability and counteract the expected decline in the collision cross section.

The $^3\Pi$ state of the CH^+ product becomes accessible at 1.54 eV by reaction (4). Evidence for production of $CH^+(a\ ^3\Pi)$ has been found in examinations of product velocity distributions at a laboratory angle of 0° by Koski and co-workers.[43] While these authors did not attempt to quantify the fraction of triplet state produced, an examination of the velocity distributions (Fig. 1 in Ref. 43) suggests that it is at least 5% and could be as large as 30% at a relative energy of 2 eV. Since the electronic states are not completely resolved and the $^3\Pi$ state overlaps with vibrationally excited ground state products, no precise value can be obtained from 0° velocity distributions such as these. Nevertheless, the $^3\Pi$ product channel could significantly contribute to the total reaction cross section. The present experiments do not provide any unambiguous evidence for or against the production of the $^3\Pi$ state. However, the fact that the cross sections do not decline above 1 eV as predicted by the simple ion–induced dipole model may imply that $^3\Pi$ is contributing significantly. Also, the intramolecular isotope branching ratio for reaction with HD appears to have a break near the 1.5 eV threshold for production of $CH^+(^3\Pi)$ (Fig. 5). This is further circumstantial evidence for a new reaction pathway beginning in this region. The $^3\Pi$ channel will be discussed further in relation to phase space theory in paper II.

Higher excited product channels, reactions (5)–(7), become accessible in the 3 to 5 eV region. Reaction (5), formation of $CH^+(A\ ^1\Pi)$, has been observed from $C^+(^2P) + H_2$ collisions in chemiluminescence experiments.[18,44–46] The cross section for reaction (5) rises from the 3.4 eV threshold to a maximum near 5 eV. The estimated magnitude of the cross section, however, is only $\sim 2\%$ of the total reaction cross section.[47] The process is improbable because formation of $CH^+(A\ ^1\Pi)$ from ground state reactants requires several crossings of potential energy surfaces.[47] Reactions (6) and (7) are expected to be unlikely for the same reason and have not been observed experimentally. Chemiluminescence from $CH(^2\Delta)$, which can be formed above 6.3 eV, has been observed but is an order of magnitude smaller than $CH^+(A\ ^1\Pi)$ chemiluminescence.[47] Because of their small magnitude, the presence of these higher excited channels does not substantially affect the shapes of the total excitation functions.

HIGH ENERGY FALLOFF

Following the plateau region, the cross sections for reactions (1) through (3) decrease sharply starting at about 4.5 eV. As this energy matches the endothermicity for process (9), this is compelling through indirect evidence for the onset of the dissociation of the putative CH^+ (CD^+) products. The fact that the decline in the cross section commences at the thermochemical threshold for dissociation indicates that there are strong interactions between all three atoms, allowing energy to be partitioned into the breaking of the diatomic chemical bond. If the mechanism were entirely direct, say in the spectator stripping limit,[48] process (9) could not occur until higher energies because some of the energy would be tied up as translational energy of the $CH^+ + H$ products. The spectator stripping model critical energies, below which the diatomic product remains bound and above which it has too much internal energy and dissociates, are 9.1 eV for reaction (1), 8.6 eV for reaction (2), 12.7 eV for reaction (3a), and 6.9 eV for reaction (3b). The cross sections decrease with increasing energies up to 15 eV c.m., but there are no sharp breaks in the cross sections at these spectator stripping critical energies. This shows that spectator stripping is not the dominant process; rather, products are formed with a broad distribution of translational and internal energies.

The observed intramolecular isotope effect further supports this picture. The isotope branching ratio for reaction with HD, Fig. 5, begins increasing (toward favoring CH^+) at about 4.5 eV, the threshold for the process $C^+ + HD \rightarrow C^+ + H + D$. This break in the intramolecular isotope ratio as well as the falloff of the total cross sections indicates the onset of production dissociation, which as discussed above requires strong interactions among all three atoms near its threshold. A further increase in the slope of the branching curve occurs around 7 eV, close to the spectator stripping critical energy ($E_s = 6.9$ eV) for production of CD^+. In the spectator stripping model, the liberated H and D atoms have nearly the same velocities and therefore the D atom carries away twice as much translational energy as H, thus stabilizing the CH^+ diatom against dissociation relative to CD^+. Therefore, the CH^+ product is strongly favored for stripping mechanisms at high energies. Simple spectator stripping cannot be the dominant mechanism, however, since the CD^+ cross section would then go to zero at $E_s(CD^+) = 6.9$ eV and no products would be observed above $E_s(CH^+) = 12.7$ eV. This is clearly not the case, even when energy broadening is considered (Fig. 5).

This interpretation anticipates and is consistent with information about the dynamics of the reaction from the differential cross section measurements of Mahan and Sloane[17] and of Koski and co-workers.[49] At high energies, the reactive scattering for H_2 and D_2 becomes increasingly asymmetric and forward peaked. The velocity of the forward peak, however, does not correspond with the spectator stripping model and there is an appreciable amount of wide angle scattering at all energies.[17] The differential reactive scattering from $C^+ + HD$ becomes increasingly asymmetric (slight forward peaking) with increasing energy, CH^+ more so than CD^+.[17] These observations indicate that while the mechanism does become increasingly impulsive at high energies, there remain strong interactions among all three atoms.

REACTION RATES

Energy-dependent rate

The cross sections $\sigma(E)$ from the guided beam experiment may alternatively be presented as an energy dependent reaction rate. The phenomenological rate constant is $k(E') = \sigma(E) \cdot v$, where $v = (2E/\mu)^{1/2}$ is the nominal center-of-mass velocity, $\mu = mM/(m+M)$ is the reduced mass of the reactants, m is the ion mass, and M is the mass of the target gas. The mean relative energy of the reactants, taking into account the thermal motion of the target gas, is $E' = E + (3/2)\gamma k_B T$, where $\gamma = m/(m+M)$ and T is the target gas temperature.[15] Figure 7 shows $k(E')$ for all three isotopic $C^+ + H_2$ reactions. The data are the same as in Figs. 1–3. The intermolecular isotope effect is emphasized for the rate constants compared to the cross sections due to the dependence of the relative velocity on the reduced mass of the reactants.

The $\sigma(E)$ presentation of the results is generally preferable since the $k(E')$ calculation amplifies possible errors in the ion energy determination. However, the phenomenological rate constant $k(E')$ is equivalent to hyperthermal rate constants obtained by flow/drift tube methods and Fig. 7 is included to allow comparison to such results. Adams, Smith, and Millar measured the rate of reaction (1) using selected ion flow/drift tube techniques.[50] They report that the rate rises from 6.1×10^{-12} $cm^3\,s^{-1}$ at 0.23 eV to 3×10^{-11} $cm^3\,s^{-1}$ at 0.46 eV. As shown in Fig. 7, the lower energy

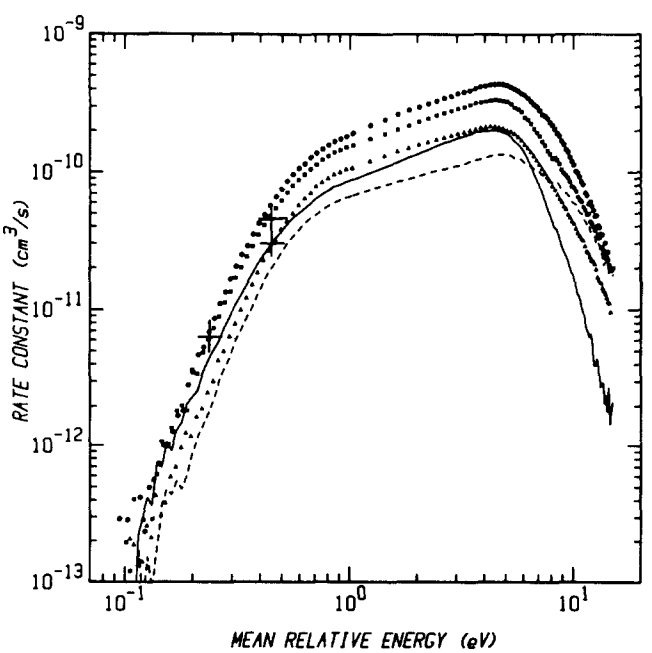

FIG. 7. Phenomenological rate constants as a function of the mean relative kinetic energy of the reactants. The data are the same as the cross section results presented in Figs. 1, 2, and 3, but have been converted to rate constants as described in the text. The symbols denote the total reaction rates: circles, reaction (1); triangles, reaction (2); squares, reaction (3). The lines give the individual product channels for reaction with HD: solid line, CD^+ [reaction (3b)], and dashed line, CH^+ [reaction (3a)]. The large crosses show the flow/drift tube data of Refs. 50 and 51 for reaction (1).

value agrees well with the present work, but at the higher energy, their rate is about a factor of 2 smaller.[51] Both beam and flow/drift tube experiments suffer from difficulties in extracting the true cross sections or rate constants from the energy-broadened experimental results. The major experimental difference between the two methods involves the translational and internal energy distributions. Under the single collision conditions of the guided beam experiments, the ion kinetic energy is well defined by a displaced Boltzmann distribution[15,28] and the internal energies are determined by ion source conditions and the temperature of the target gas. In high-pressure flow/drift tube experiments, the ion kinetic energies are controlled by interactions with the bath gas and internal energies can be influenced by the hyperthermal ions. In reaction (1), the rate constant in the threshold region is very sensitive to the actual energy distribution. The discrepancy between the rate constants suggests that the mean kinetic energy in the flow/drift tube experiment is actually lower than 0.46 eV at the higher point. Errors in the rate constant magnitudes could also explain some of the discrepancy.[51]

Thermal rate constant

In the limit of zero ion energy, the experimental rate $k(E')$ is equal to the thermal rate constant $k(T')$, where $T' = \gamma \cdot T$ is the effective temperature.[15] While clearly less than 10^{-13} cm^3 s^{-1}, the thermal rate constant for reactions (1)–(3) is too small to be determined directly by this means. Alternatively, the thermal rate constant may be determined from the true (unconvoluted) cross section by the relationship

$$k(T) = (1/\pi\mu)^{1/2} \cdot (2/k_B T)^{3/2} \cdot \int_0^\infty \sigma(E) \cdot E \cdot \exp(-E/k_B T) \cdot dE. \quad (11)$$

To eliminate the effects of the experimental energy broadening of the threshold, the empirical fits of $\sigma(E)$ in Table II are used in Eq. (11) up to 1 eV and the data is integrated directly at higher energies (where the energy broadening is less pronounced). Table III lists the average values of $k(T)$ at 300 K obtained for each isotopic reaction. The various empirical fits result in values of $k(T)$ which vary by 10% (1 std. dev.) for reactions (1) and (2) and 40% for reactions (3a) and (3b). Considering also the experimental uncertainties in the magnitude of $\sigma(E)$ and the errors involved in the application of Eq. (11), we estimate the derived thermal rates have uncertainties of at least 50% and conservatively a factor of 2. Table III also lists rate constants obtained from phase space theory (paper II) which agree quite well with the experimental values.

A simple treatment[52] for estimating rates of endothermic ion molecule rates is given by

$$k_{endo} \sim (k_c/2) \cdot \exp(-\Delta H^\circ/k_B T). \quad (12)$$

This assumes that a thermoneutral reaction would proceed at half the collision rate k_c and that endoergic reactions are further reduced by the Boltzmann energy factor. The collision rate may be calculated by the Langevin model and ΔH° is given by $\langle E_T \rangle$. Rates estimated this way are listed in Table III. These rates are uniformly higher than experiment. The agreement is greatly improved if the rates are further reduced by 1/3 to account for the fraction of reactant potential energy surfaces which are known to be accessible according to *ab initio* calculations.[1–4] The success of the comparison (Table III) validates the use of this very simple treatment to estimate order-of-magnitude rates for endothermic ion–molecule reactions. However, knowledge of the potential energy surfaces and possible energy barriers is essential to obtain reliable estimates.

TABLE III. Thermal rate constants.[a]

Reaction	k_{exp}[b]	k_{ps}[c]	k_{endo}[d]	$k_{endo}/3$
(1) $C^+ + H_2 \rightarrow CH^+ + H$	12	10	38	13
(2) $C^+ + D_2 \rightarrow CD^+ + D$	2.3	2.7	6.3	2.1
(3a) $C^+ + HD \rightarrow CH^+ + D$	2	1.0	3.0[e]	1.0[e]
(3b) $C^+ + HD \rightarrow CD^+ + H$	10	7.8	18[e]	6[e]

[a] At 300 K, in units of 10^{-17} cm^3 s^{-1}.
[b] This work; derived from experimental cross sections (see the text). Estimated uncertainty is a factor of 2.
[c] Phase space theory, Ref. 16.
[d] Equation (12) in the text.
[e] Reduced by 1/2 to account for CH^+/CD^+ branching.

Thermal rates for endothermic reactions are controlled by the overlap of the high energy part of the Maxwell–Boltzmann energy distribution with the threshold cross section. This is illustrated by Eq. (12) for k_{endo}, which shows that the magnitude of the rate constant is determined mainly by the endoergicity. Therefore, the agreement of the rates derived experimentally via Eq. (11) with k_{endo} just reflects the observation that these reactions proceed at their thermochemical thresholds without a delayed onset. $k(T)$ in Eq. (11) and $k_c \cdot \exp(-\Delta H^\circ/k_B T)$ are mathematically equivalent for a cross section of the form given by Eq. (8) with $n = 0.5$, $m = 1$, and $E_T = \Delta H^\circ$, the form predicted by a simple ion–induced dipole model.[31]

SUMMARY

Guided ion beam methods have been used to obtain accurate integral cross sections for the reactions of C^+ with H_2, HD, and D_2 to form CH^+ or CD^+. The quality of the data represents a marked improvement over previously published total cross sections for this system. In particular, ambiguities in previous studies involving the energy scale have been eliminated. The wide translational energy range, from threshold to about 15 eV c.m., and the examination of kinetic isotope effects allows detailed comparison to simple reaction models and to theoretical treatments of the reaction dynamics. It is hoped that these results will encourage further theoretical work on this important system.

The true cross sections rise very sharply from the thermochemical threshold energies. This indicates there is no barrier in excess of the reaction endothermicity, in agreement with features of the potential energy surfaces known from theoretical studies. Further analysis of the threshold energies and threshold behavior leads to the conclusion that the higher populated rotational states of the reactant diatom are at least as reactive as the ground rotational state. The

results may also be consistent with a moderate degree of rotational enhancement in the reaction probability. No direct measurements of the rotational dependence of the cross sections are available.

The energy resolution of the cross section measurements is sufficient to resolve shifts in the threshold energies among the isotopic variants of the reaction, which are caused by the zero-point vibrational energy differences of the reaction endothermicities. For reaction with HD, the difference in endoergicity for production of CH^+ vs CD^+ results in a large intramolecular isotope effect very near the threshold.

The total cross sections exhibit an unexpected *inter*molecular isotope effect. The relative shape of the cross sections are very similar, but the magnitudes have the dependence $\sigma(H_2) > \sigma(HD) > \sigma(D_2)$. As no model explaining this observation has been advanced, theoretical investigation of this effect would be useful.

The total cross sections are remarkably flat in the 1 to 4 eV region, while a simple model based on the ion–induced dipole potential predicts a decline following the threshold region. The intramolecular isotope effect for reaction (3) shows increasing production of CD^+ with increasing energy in this region. These observations suggest that new reaction channels add to the reaction probability in this region. One likely possibility is the $^3\Pi$ excited state of CH^+, which can be formed above ~ 1.5 eV.

Above the 4.5 eV threshold for dissociation of the diatomic products, the cross section for formation of these products drops rapidly. In addition, the intramolecular isotope effect for reaction of HD begins to strongly favor the CH^+ product. The results are in agreement with the differential reactive scattering measurements of Mahan and Sloane,[17] which show that the reaction mechanism becomes increasingly direct at high energies but that there remain strong interactions among all three nuclei.

ACKNOWLEDGMENTS

We gratefully acknowledge helpful discussions with D. Gerlich and E. E. Ferguson. We thank Ch. Schlier for providing Ref. 37. This research was funded by the National Science Foundation, Grant No. CHE-8306511.

[1] D. H. Liskow, C. F. Bender, and H. F. Schaefer III, J. Chem. Phys. **61**, 2507 (1974).
[2] P. K. Pearson and E. Roueff, J. Chem. Phys. **64**, 1240 (1976).
[3] C. W. Bauschlicher, Jr. and I. Shavitt, Chem. Phys. Lett. **75**, 62 (1980).
[4] I. Kusunoki, S. Sakai, S. Kato, and K. Morokuma, J. Chem. Phys. **72**, 6813 (1980).
[5] D. G. Truhlar, J. Chem. Phys. **51**, 4617 (1969).
[6] E. Herbst and S. K. Knudson, Chem. Phys. **55**, 293 (1981).
[7] (a) D. A. Webb and W. J. Chesnavich, J. Phys. Chem. **87**, 3791 (1983); (b) W. J. Chesnavich, V. E. Akin, and D. A. Webb, Astrophys. J. **287**, 676 (1984).
[8] J. P. Sullivan and E. Herbst, Chem. Phys. Lett. **55**, 226 (1978).
[9] M. Gonzalez, A. Aguilar, and J. Virgili, Chem. Phys. Lett. **113**, 187 (1985); M. Gonzalez and A. Aguilar, *ibid.* **118**, (1985).
[10] E. Herbst and S. K. Knudson, Astrophys. J. **245**, 529 (1981); R. E. White, *ibid.* **284**, 695 (1984).
[11] K. M. Ervin and P. B. Armentrout, J. Chem. Phys. **80**, 2978 (1984).
[12] W. D. Maier, J. Chem. Phys. **46**, 4991 (1967).
[13] (a) E. Lindemann, L. C. Frees, R. W. Rozette, and W. S. Koski, J. Chem. Phys. **56**, 1003 (1972); (b) L. C. Frees, P. L. Pearl, and W. S. Koski, Chem. Phys. Lett. **63**, 108 (1979).
[14] (a) P. F. Fennelly, Ph.D. thesis, Brandeis University, 1972; P. F. Fennelly, M. J. Henchman, A. S. Werner, and J. F. Paulson (unpublished, 1972).
[15] K. M. Ervin and P. B. Armentrout, J. Chem. Phys. **83**, 166 (1985).
[16] K. M. Ervin and P. B. Armentrout, J. Chem. Phys. **84**, 6750 (1986).
[17] B. H. Mahan and T. M. Sloane, J. Chem. Phys. **59**, 5661 (1973).
[18] I. Kusunoki and Ch. Ottinger, J. Chem. Phys. **73**, 2069 (1980).
[19] H. Helm, P. C. Cosby, M. M. Graff, and J. T. Moseley, Phys. Rev. A **25**, 304 (1982).
[20] B. H. Mahan and A. O'Keefe, Chem. Phys. **69**, 35 (1982).
[21] A. Carrington and D. A. Ramsay, Phys. Scr. **25**, 272 (1982).
[22] R. P. Saxon, K. Kirby, and B. Liu, J. Chem. Phys. **73**, 1873 (1980); B. Levy, J. Ridard, and E. LeCoarer, Chem. Phys. **92**, 295 (1985).
[23] E. Teloy and D. Gerlich, Chem. Phys. **4**, 417 (1974).
[24] (a) K. M. Ervin, S. K. Loh, N. Aristov, and P. B. Armentrout, J. Phys. Chem. **87**, 3593 (1983); (b) P. B. Armentrout, S. K. Loh, and K. M. Ervin, J. Am. Chem. Soc. **106**, 1161 (1984); (c) J. L. Elkind and P. B. Armentrout, J. Phys. Chem. **88**, 5454 (1984); (d) N. Aristov and P. B. Armentrout, J. Am. Chem. Soc. **106**, 4065 (1984); (e) J. L. Elkind and P. B. Armentrout, J. Phys. Chem. **89**, 5626 (1985).
[25] H. M. Rosenstock, K. Draxl, B. W. Steiner, and J. T. Herron, J. Phys. Chem. Ref. Data **6**, Suppl. 1 (1977).
[26] C. E. Moore, Natl. Stand. Ref. Data Ser., Natl. Bur. Stand. **1**, No. 35 (1970).
[27] P. A. M. Van Koppen, P. R. Kemper, A. J. Illies, and M. T. Bowers, Int. J. Mass Spectrom. Ion Proc. **54**, 263 (1983).
[28] P. J. Chantry, J. Chem. Phys. **55**, 2746 (1971).
[29] C. Lifshitz, R. L. C. Wu, T. O. Tiernan, and D. T. Terwilliger, J. Chem. Phys. **68**, 247 (1978).
[30] R. D. Levine and R. B. Bernstein, *Molecular Reaction Dynamics* (Oxford University, New York, 1974), p. 46.
[31] R. D. Levine and R. B. Bernstein, J. Chem. Phys. **56**, 281 (1972).
[32] W. J. Chesnavich and M. T. Bowers, J. Phys. Chem. **83**, 901 (1979).
[33] In the convolution, the ion energy distribution is assumed Gaussian with the measured width. To check this approximation, convolutions over the measured ion energy distribution sampled at ten points were performed. The resulting convoluted function was virtually identical. The broadening by the thermal motion of the target gas is much greater than that due to the ion energy spread.
[34] In our preliminary report, Ref. 11, the single integral approximation of Lifshitz *et al.*, Ref. 29, was used inappropriately. Using the exact convolution changes somewhat the shape of the convoluted model cross section, but does not alter the conclusions made in the comparison to the data.
[35] G. E. Forsythe, M. A. Malcom, and C. B. Moler, *Computer Methods for Mathematical Computations* (Prentice-Hall, Englewood Cliffs, N. J., 1977), p. 102.
[36] An exception is that the cross sections of Koski and co-workers, Ref. 13(a), for reactions (1) and (2) diverge widely from our data and other reports. Both the apparent threshold (see Ref. 11) and the high energy falloff occur at higher energies in the Koski data. Later work on the threshold region of reaction (1) by the same group, Ref. 13(b), is in general agreement with the present results once an energy scale correction is eliminated. Reference 13(a) does not provide any indications as to possible sources of the discrepancy.
[37] D. Cahnbley, Diplomarbeit, Universität Freiburg, 1982; Ch. Schlier (private communication).
[38] D. Gerlich, XIV Int. Conf. Phys. Elec. Atomic Collisions, Palo Alto, California, 1985.
[39] Gerlich's absolute magnitudes are determined by calibration with the $Ar^+ + H_2$ reaction cross section measured on the Teloy and Gerlich, Ref. 23, guided beam apparatus [D. Gerlich (private communication)]. A comparison of results for that reaction with data from this laboratory, Ref. 15, shows a deviation of $14 \pm 2\%$ in the same direction.
[40] D. Gerlich (private communication).
[41] An alternative assumption is that $E_T = \Delta H^\circ_0$ but $E = E_{rel} + E_{int}$, i.e., the denominator of Eq. (8) is the total energy rather than the kinetic energy. Since the internal energies are relatively small, either form gives identical results within the uncertainty of the fitting procedure for the present case.
[42] N. Sathyamurthy, Chem. Rev. **83**, 601 (1983).
[43] C. A. Jones, K. L. Wendell, and W. S. Koski, J. Chem. Phys. **66**, 5325 (1977).

[44]H. H. Harris, M. G. Crowley, and J. J. Leventhal, Phys. Rev. Lett. **34**, 67 (1975).
[45]J. Appell, D. Brandt, and Ch. Ottinger, Chem. Phys. Lett. **33**, 131 (1975).
[46]I. Kusunoki and Ch. Ottinger, J. Chem. Phys. **71**, 4227 (1979).
[47]Ch. Ottinger, in *Electronic and Atomic Collisions*, edited by G. Watel (North-Holland, Amsterdam, 1978), pp. 639–661.
[48]A. Henglein and K. Lacmann, Adv. Mass Spectrom. **3**, 331 (1966); A. Henglein, in *Ion–Molecule Reactions in the Gas Phase*, edited by P. J. Ausloos (American Chemical Society, Washington, 1966), p. 63; A. Ding, K. Lacmann, and A. Henglein, Ber. Bunsenges. Phys. Chem. **71**, 596 (1967).
[49]C. R. Iden, R. Liardon, and W. S. Koski, J. Chem. Phys. **54**, 2757 (1970); **56**, 851 (1972).
[50]N. G. Adams, D. Smith, and T. J. Millar, Mon. Not. R. Astron. Soc. **211**, 857 (1984).
[51]N. G. Adams and D. Smith have since repeated the measurement at 0.46 eV and find $k = 4.5 \times 10^{-11}$ cm^3 s^{-1} ($\pm$ 40%), which is in better agreement with the present results. [D. Smith (private communication, 1985).]
[52]D. Smith and N. G. Adams, J. Phys. Chem. **89**, 3964 (1985).